Eur. Phys. J. D **39**, 141–155 (2006)
DOI: 10.1140/epjd/e2006-00072-8

THE EUROPEAN PHYSICAL JOURNAL D

Electron density changes and high harmonics generation in H_2 molecule under intense laser fields

A. Wadehra[1,a] and B.M. Deb[2,b]

[1] Department of Chemistry, Panjab University, 160014 Chandigarh, India
[2] S.N. Bose National Centre for Basic Sciences, J.D. Block, Sector III, Salt Lake, 700098 Kolkata, India
and
Jawaharlal Nehru Centre for Advanced Scientific Research, Jakkur, 560064 Bangalore, India

Received 3rd October 2005 / Received in final form 16 January 2006
Published online 4 April 2006 –

Abstract. Under interaction with a high-intensity laser field, the real-time femtosecond dynamics of the electron density in the H_2 molecule has been studied quantum mechanically. For this purpose, a time-dependent generalized nonlinear Schrödinger equation of motion, developed earlier in our laboratory by combining density functional theory and quantum fluid dynamics in real space, is solved numerically at the equilibrium internuclear distance of the molecule. By employing various time-dependent calculated properties as probes, information and insight are obtained about the phenomena of excitation, ionization, bond-softening, dipole formation and high-harmonics generation. The present approach goes beyond the linear response formalism.

PACS. 33.80.-b Photon interactions with molecules – 42.50.Hz Strong-field excitation of optical transitions in quantum systems; multiphoton processes; dynamic Stark shift – 42.65.Ky Frequency conversion; harmonic generation, including higher-order harmonic generation

1 Introduction

The active interplay of theoretical investigations and experimental developments has uncovered a new domain in the physics of laser-matter interactions. Not only are these studies important from a fundamental point of view, they also have multiple applications in science and technology. In such strong-field processes, the strength of the driving laser field approaches and exceeds the strength of internal binding forces in the irradiated quantum system. Since the applied field is a large perturbation, it modifies the internal structure of the system and significantly alters its decay dynamics. Consequently, the perturbative expansions break down and non-perturbative theoretical treatments are required to describe adequately the interaction of real systems and intense lasers. An entirely unknown realm of physics is thus thrown open to investigation whereby a host of counter-intuitive nonlinear phenomena has been discovered. The mechanism of laser-atom interactions has been explored extensively and is understood to a large extent. However, interest is now shifting to study molecules but this area of research is still in its infancy [1–3]. Molecules have a higher level of complexity than atoms because of the additional degrees of freedom associated with the nuclear motion. An enormous computational effort is required to treat electronic and nuclear degrees of freedom on an equal footing which makes an accurate treatment of the dynamical behaviour of even the simplest neutral molecule, H_2, in intense laser fields quite challenging. It often becomes essential to consider the different time-scales of response of electronic and nuclear motion; the latter can thus be neglected (adiabatic or Born-Oppenheimer approximation). Within this approach, the nuclei are treated as fixed and the response of an electron to the external field is essentially instantaneous on the time-scales of both the nuclear motion and the optical period of the laser field. Various avenues have been explored to probe molecular dynamics and a wealth of interesting processes such as multiphoton ionization [4,5], above-threshold ionization (ATI) [6,7], above-threshold dissociation (ATD) [8–11], alignment with external fields [12,13], high harmonics generation (HHG) [14–21], ionization that depends on internuclear separation [22,23], dissociation through bond-softening [10,24,25] and Coulomb explosion [17,26–28] have been studied.

Several theoretical time-dependent approaches have evolved for obtaining insights into these nonlinear multiphoton phenomena arising out of interactions between

[a] *Present address*: Department of Physics, Ohio State University, Columbus, OH 43210, USA.
[b] e-mail: bmdeb@yahoo.co.in

high intensity lasers and small molecules. Not surprisingly, most of these are restricted to one-electron hydrogen molecular ion and the simplest two-electron neutral H_2 molecule. One of these treatments employed a finite element method, which includes both bound and continuum states, to solve the time-dependent Schrödinger equation (TDSE) in three-dimensional Cartesian coordinates for obtaining ionization rates and HHG spectra [20]. Treating the nuclei as fixed, the mechanism of enhanced ionization has been analyzed through solving TDSE for reduced dimensionality models [22,29], a 3D fully-correlated ab initio method [23,25] which also accounts for bond-softening, and an accurate evaluation of 3D two-electron wavepacket dynamics by the dual transformation method [30]. A modified split-operator technique has been applied to solve TDSE for H_2 with moving nuclei with an effort to understand strong-field ionization dynamics [31]. The phenomenon of HHG has also been examined by employing TDDFT and including optimized effective potential along with a self-interaction correction for the exchange-correlation potential and obtaining the solution through the time-dependent pseudospectral method [19] and in another study by including nuclear dynamics to also observe Coulomb explosion and laser-induced photodissociation [32]. A non-adiabatic quantum molecular dynamics approach [33] has also been developed to analyze HHG in H_2 molecule with both fixed and dynamic nuclei by using linearly polarized laser pulses. Another application of the split-operator method has been to solve the TDSE and obtain single- as well as double-ionization probabilities and HHG spectra for the first three electronic states of H_2 [21]. A recent paper employed linear combination of atomic orbitals (LCAO) and molecular orbital (MO) method in addition to the strong field approximation, wherein nuclear motion is also considered for H_2 molecule, to study ionization rates, photoelectron spectra and angular distributions [34].

However, it appears that the role of density as a valuable tool to tackle the computational difficulties within time-dependent quantum mechanical formulations and elucidate the nature of such nonlinear dynamics has not been understood or exploited to its potential. This is all the more important because realistically much of the dynamical phenomena in atoms and molecules, including those phenomena associated with exchange and correlation effects, can be viewed as originating from the displacement of electron density from one spatial region to another (note that in the quantum fluid dynamical approach [35] to many-electron systems one requires both the electronic charge density and current density for complete information). For example, ionization is associated with the removal of density in regions far away from the nuclei; excitation with the removal of electron density from the nuclear region; bond-softening with the depletion of density in the binding region while dissociation can be visualized as a consequence of increased depletion of density in the binding region and consequent separation of the two nuclei. Thus, it becomes essential to follow the dynamical changes of electron density in a molecule in order to fully understand its behaviour in such strong external fields. For this purpose, we have adopted a non-perturbative, time-dependent quantum fluid density functional method [35–39] that is an amalgamation of density functional theory (DFT) and quantum fluid dynamics (QFD), permits the use of a "classical" language within quantum mechanics and may have certain advantages over other approaches. Successful applications of this method have already been made in the intense laser-atom dynamics [40–42].

The present study deals with the direct interaction between the electron cloud of the molecule and the laser photons. We assume here that the two nuclei are fixed in space at the equilibrium internuclear distance, $R_{eq} = 1.4$ a.u and perform a thorough analysis of the three-dimensional electron dynamics. A question arises whether it is worthwhile to restrict this study to R_{eq} only and not explore other internuclear separations. The following discussion justifies our interest. Although the calculations with fixed internuclear distance R for both 1D [22] and 3D [23] H_2 have exhibited a strong enhancement of ionization rate at internuclear separations in the range from $R = 3-10$ a.u, whether the molecule actually probes such large separations in reality is still an unanswered question. So far there has been no experimental observation of enhanced ionization in this molecule. It seems difficult to verify this theoretical finding experimentally because the multiphoton ionization of H_2 occurs at equilibrium geometry much before it has the opportunity to expand towards larger internuclear distances. Moreover, it was concluded in a one-dimensional study on a model H_2 molecule beyond Born-Oppenheimer treatment that the internuclear distance of a neutral molecule even under intense lasers (laser intensity $\sim 10^{14}$ W cm^{-2}) remains close to the equilibrium internuclear distance and that the molecule predominantly decays due to ionization without showing any signature of dissociation [31]. Furthermore, it was reported that the dynamics of the molecule in such a field is essentially dominated by the ionization rates near the equilibrium geometry. Also, the molecular core is considered as frozen here because the orientation of molecules cannot change in the time scale of short femtosecond laser pulses. Such a fixed-nuclei treatment implies ignoring dissociation and Coulomb explosion but there is not much to lose because considering the intensities employed in this paper these processes do not contribute significantly to the decay as compared to ionization that plays a lead role. Moreover, the laser field affects electron dynamics to a much larger extent than nuclei which are considerably heavier than electrons and consequently their motion is relatively quite slow. It is thus clear that a thorough exploration of this molecule with fixed nuclei and at the equilibrium internuclear separation is a worthwhile step towards comprehending the nature of dynamical evolution.

The present work is not only an attempt to examine the suitability of TDQFDFT to the study of dynamical processes in molecules but also an effort to obtain a deeper understanding and finer details of the phenomena observed in terms of density-based time-dependent

quantities. This is an extension of the previous work done in our laboratory on two-electron molecules [43,44] which was computationally limited to a rather short period of time as well as small computation grid and therefore could not reproduce HHG accurately.

The layout of this paper is as follows: Section 2 lays down the numerical method of calculating the time-dependent density directly. Section 3 lists different TD quantities required to visualize the phenomena arising out of the interaction, interprets the results and compares with the already existing literature. Section 4 makes certain concluding remarks on the validity of this method and scope for future investigations in this direction.

2 Method of calculation

The detailed methodology of TDQFD, its association with DFT and the generation of GNLSE for calculating the time-dependent density arising out of interaction of the system with and external TD field have been discussed in the earlier works done in our research group [35–39]. The hydrodynamic formulation is closer to the classical description of quantum systems in the sense that the reduction of 3N degrees of freedom in the Schrödinger wavefunction to 3 in the hydrodynamical "wavefunction" leads to a loss of interference which is a characteristic feature of quantum systems Therefore, the hydrodynamical "wavefunction" may be regarded as a reduced form of the Schrödinger wavefunction.

The Schrödinger-like equation of motion, obtained through a hydrodynamical continuity equation and an Euler-type equation, is given by (atomic units employed throughout this paper)

$$\left[-\frac{1}{2}\nabla^2 + V_{\mathit{eff}}([\rho];r,t)\right]\Psi(r,t) = i\frac{\partial\Psi(r,t)}{\partial t} \tag{1}$$

where Ψ is the hydrodynamical "wavefunction"; density, $\rho(r,t) = |\Psi(r,t)|^2$, and the effective potential $V_{\mathit{eff}}([\rho];r,t)$, containing both classical and quantum terms, is defined as

$$V_{\mathit{eff}}([\rho];r,t) = \frac{\delta E_{el-el}}{\delta\rho} + \frac{\delta E_{nu-el}}{\delta\rho} + \frac{\delta E_{xc}}{\delta\rho} + \frac{\delta E_{corr}}{\delta\rho} + \frac{\delta E_{ext}}{\delta\rho}. \tag{2}$$

Equation (1) is a generalized nonlinear Schrödinger equation [38,45] (GNLSE) since V_{eff} depends on $\Psi(r,t)$; it is different from the usual nonlinear Schrödinger equation which is cubic in $\Psi(r,t)$. The various terms comprising $V_{\mathit{eff}}([\rho];r,t)$ are as follows: E_{el-el} is the interelectronic repulsion term, E_{nu-el} is the electron-nuclear attraction term, E_{xc} is the exchange and correlation energy functional, E_{corr} arises from a non-classical correction term added to the Weizsaecker kinetic energy required for more than two-electron systems (this term vanishes for a one-electron system and a two-electron Hartree-Fock system; in the present case of H_2 molecule, this correction term is neglected); E_{ext} is the interaction energy between the electrons and the external field. In other words,

$$E_{el-el} = \frac{1}{2}\iint \frac{\rho(r,t)\,\rho(r',t)}{|r-r'|}dr\,dr'$$
$$\frac{\delta E_{el-el}}{\delta\rho} = \int \frac{\rho(r',t)}{|r-r'|}dr' \tag{3}$$
$$E_{nu-el} = -\int \frac{Z}{r}\rho(r,t)\,dr$$
$$\frac{\delta E_{nu-el}}{\delta\rho} = -\frac{Z}{r}. \tag{4}$$

Taking E_{xc} as $E_x + E_c$, various exchange and correlation functionals are available in the literature. However, we have employed a local exchange functional [46]

$$E_x = E_x^{LDA} - C_x\int \frac{\rho^{1/3}}{\left(1 + r^2\rho^{2/3}/\alpha_x\right)}\rho\,dr$$
$$E_x^{LDA} = -C_x\int \rho^{4/3}dr$$
$$C_x = \frac{3}{4}\left(\frac{3}{\pi}\right)^{1/3}, \quad \alpha_x = 0.0244$$
$$\frac{\delta E_x}{\delta\rho} = \frac{\delta E_x^{LDA}}{\delta\rho} - C_x\left[\frac{\frac{4}{3}\rho^{1/3} + \frac{2}{3}\frac{r^2\rho}{\alpha_x}}{\left(1 + \frac{r^2\rho^{2/3}}{\alpha_x}\right)^2}\right]$$
$$\frac{\delta E_x^{LDA}}{\delta\rho} = -\frac{4}{3}C_x\rho^{1/3}. \tag{5}$$

Correlation effects have been included by using a simple, local parameterized Wigner-type functional [47]

$$E_c = -\int \frac{\rho}{a + b\rho^{-1/3}}dr$$
$$\frac{\delta E_c}{\delta\rho} = -\frac{a + c\rho^{-1/3}}{\left(a + b\rho^{-1/3}\right)^2} \tag{6}$$

where $a = 9.81$, $b = 21.437$, and $c = 28.582667 = (4/3)b$. It may be noted that since the present calculations neglect E_{corr}, for a two-electron system equation (1) reduces to the time-dependent (TD) Kohn-Sham equations [37]. However, for other many-electron systems, E_{corr} cannot be neglected and the single equation, equation (1), remains valid for all of these systems (see also Ref. [48]) for the direct calculation of TD electron density and other properties.

We have limited our calculations to the case where the internuclear axis is aligned parallel to the direction of laser polarization. It has been shown that molecules with the outermost orbital symmetry as σ_g show maximum HHG yield when they are aligned along the laser direction whereas for those with outermost π_g orbitals HHG yield is the highest when they are aligned at about 45° from the polarization axis [13]. The laser electric field propagating

along the molecular $\tilde{z}$-axis is treated classically

$$E_{ext} = -\int E(t)\,\tilde{z}\rho(r,t)\,dr$$
$$\frac{\delta E_{ext}}{\delta\rho} = -E(t)\,\tilde{z}$$
$$E(t) = E_0 f(t)\sin(\omega_L t) \tag{7}$$

where $E_0 = \sqrt{8\pi I/c}$; c is the speed of light, I is the intensity of laser field and the shape function of the pulse is given by

$$f(t) = \begin{cases} \dfrac{t}{t_0} & t < t_0 \\ 1 & t \geq t_0 \end{cases}. \tag{8}$$

Here, t_0 refers to the time at which the maximum value of electric field is reached, which for the present calculations is at 5 optical cycles.

The calculation of $\rho(\tilde{\rho},\tilde{z},t)$ for the hydrogen molecule is done by solving the TDGNLSE, equation (1), starting from an initial ground-state hydrodynamical density $\rho(\tilde{\rho},\tilde{z},0)$ which has been obtained as $|\Psi(\tilde{\rho},\tilde{z},0)|^2$ following the imaginary-time formulation of the TDQFD akin to the diffusion quantum Monte Carlo method (for the method adopted and its other applications see, e.g., Ref. [49] and other references therein). The ground state energy obtained with this formulation is a highly accurate value of -1.17212 a.u compared to the exact nonrelativistic value of -1.17447 [50] a.u. Since electron correlation is included, the calculated density is obviously more accurate than the ground-state Hartree-Fock density.

The formal solution of equation (1) is obtained as

$$\Psi(r,t+\Delta t) = e^{\Delta t L}\Psi(r,t).$$

Alternatively, it can be written as

$$\Psi_{l,m}^{n+1} = e^{\Delta t L}\Psi_{l,m}^{n} \tag{9}$$

where

$$L = -i\left[-\frac{1}{2}\nabla^2 + V_{\mathit{eff}}([\rho];r,t)\right]. \tag{10}$$

To describe the molecule, we choose the cylindrical coordinate system $(\tilde{\rho},\tilde{z},\phi;\ 0 \leq \tilde{\rho} \leq \infty,\ -\infty \leq \tilde{z} \leq +\infty,\ 0 \leq \phi \leq 2\pi)$ with the origin at the mid-point between the two protons. The position of the first proton, say H_A, is $R_A(0,-R_{eq}/2)$ while that of the second proton, say H_B, is $R_B(0,R_{eq}/2)$ where $R_{eq} = 1.4$ a.u is the equilibrium internuclear distance in the ground state of H_2 molecule.

Since the electron density in a diatomic molecule is cylindrically symmetric ($\tilde{\phi}$-independent), the $\partial^2/\partial\tilde{\phi}^2$ term is dropped. Thus the operator L in this coordinate system is given by

$$L = \frac{i}{2}\left[\frac{\partial^2}{\partial\tilde{\rho}^2} + \frac{1}{\tilde{\rho}}\frac{\partial}{\partial\tilde{\rho}} + \frac{\partial^2}{\partial\tilde{z}^2} + \frac{1}{\tilde{\rho}^2}\frac{\partial^2}{\partial\tilde{\phi}^2}\right] - iV_{\mathit{eff}}([\rho];\tilde{\rho},\tilde{z},t)$$
$$= \frac{i}{8x^2}\frac{\partial^2}{\partial x^2} + \frac{i}{8x^3}\frac{\partial}{\partial x} + \frac{i}{2}\frac{\partial^2}{\partial\tilde{z}^2} - iV_{\mathit{eff}}([\rho];\tilde{\rho},\tilde{z},t). \tag{11}$$

We thus have a two-dimensional system which can be discretized as

$$\tilde{\rho}_l = x_l^2;\quad 0 \leq x \leq 5.025,\quad -25.1250 \leq \tilde{z} \leq 25.1250$$
$$x_l = \delta + (l-1)\,h \qquad l = 1,2,3,\ldots,N_1$$
$$\tilde{z}_m = \tilde{z}_0 + mh \qquad m = 1,2,3,\ldots,N_2$$
$$\tilde{z}_0 = -N_2/h.$$

In our calculation, $N_1 = 51$, $N_2 = 501$, $h = 0.1005$; $\tilde{z} = -0.7035$ for nucleus A and 0.7035 for nucleus B. For best results, we have chosen $\delta = 1.0 \times 10^{-6}$, along the x-direction only; this avoids the Coulomb singularities at the nuclear sites. Furthermore, $\Delta t = 0.071643$ and 0.03582 a.u for the 1064 nm and 532 nm laser respectively, employed in this work.

We have applied the finite-difference scheme followed by Peaceman-Rachford splitting [51] and the modified Thomas algorithm [52] to solve equation (1) for obtaining the electronic density over a series of real time-steps. A suitable mask function of the form

$$\left[\cos\left\{\frac{\pi(x-x_{abs})}{2(x_{max}-x_{abs})}\right\}\cos\left\{\frac{\pi(\tilde{z}-\tilde{z}_{abs})}{2(\tilde{z}_{max}-\tilde{z}_{abs})}\right\}\right]^{3/4},$$

where $x_{abs} = 2.814$, $x_{max} = 5.025$, $\tilde{z}_{abs} = 20.100$, $\tilde{z}_{\max} = 25.125$, has been employed for $x \geq 2.814$ and $|\tilde{z}| \geq 20$, in order to avoid reflections from the grid boundaries. From the calculated densities at different times, various time-dependent properties have been calculated to obtain insights into the dynamics that are discussed in next section. Although the present methodology does not provide the conventional orbital description of the atomic/molecular system, it can nevertheless describe the dynamics arising out of the electron density distribution since the method calculates TD density directly by solving only one equation. The conceptual simplicity of the quantum fluid dynamical approach, its connections with the "classical" approaches to quantum mechanics and its high numerical accuracy in the case of real systems have been amply demonstrated before [35–41]. Furthermore, the present numerical method calculates densities in principle to *all orders of change*, beyond the linear response formalism.

3 Results and discussion

It is conceivable that a high intensity laser, such as that employed here, would lead to electron density changes either in a symmetric (identical changes around both nuclei) or an asymmetric (different changes around both nuclei) manner. There should be multiphoton excitation to higher electronic states. This can lead to ionization in the sense of density removal from the computation grid once it reaches the specified boundary far away from the nuclei. The asymmetric charge distribution around the two nuclei will eventually lead to separation of the two nuclei (possible dissociation) if the electron density evolves for a sufficiently long time in order to act as a feedback for the movement of the much heavier nuclei.

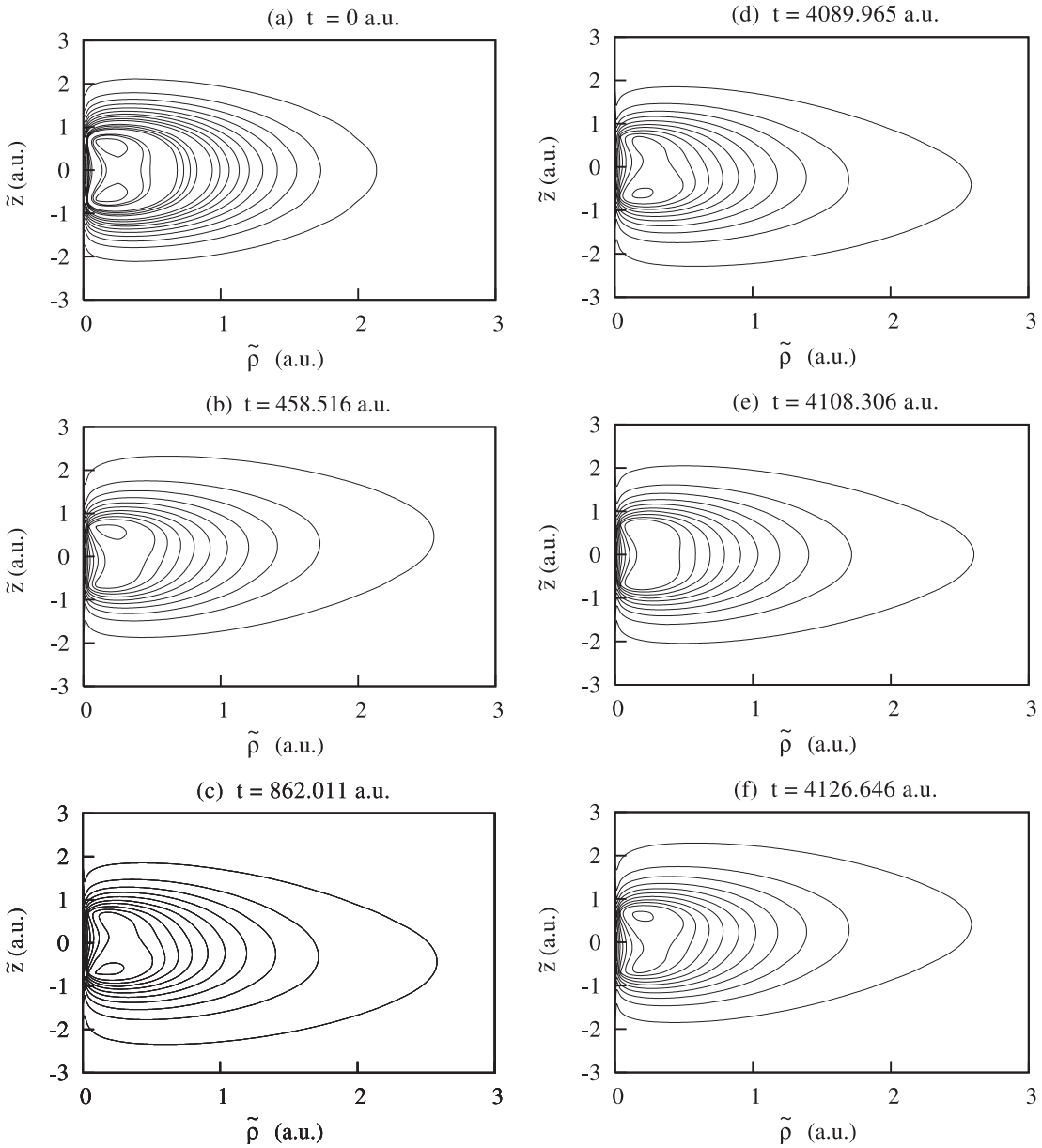

Fig. 1. Contours of time-dependent density (a.u) in the plane $(\tilde{\rho}, \tilde{z})$ for $\lambda = 532$ nm and $I = 1 \times 10^{14}$ W cm^{-2} at (a) $t = 0$, (b) $t = 458.516$, (c) $t = 862.011$, (d) $t = 4089.965$, (e) $t = 4108.306$, (f) $t = 4126.646$ a.u. The density values for the outermost and innermost contours are 0.008 and 0.22 respectively (these values are also valid for Figs. 2 and 3). The total interaction time is 100 fs, i.e., 4134.1276 a.u.

The dynamics of the interacting system are described in this paper in terms of the following properties: 3-D electron density; contours of electron density; 3-D difference density; contours of difference density; time-dependent electronic charge, $N(t)$; electronic charges around the two nuclei, $N_A(t)$ and $N_B(t)$; electronic charge around the "binding" region, $N_{BR}(t)$; electronic charges around the "antibinding" regions, $N_A^{LS}(t)$ and $N_B^{RS}(t)$; ground-state survival probability, $P_{gs}(t)$; time-dependent electric field, $E(t)$; time-dependent dipole moment, $\mu_{\tilde{z}}(t)$ and HHG spectra. The laser intensities employed for the present calculations are 1×10^{14} W cm^{-2}, 2×10^{14} W cm^{-2}, 3×10^{14} W cm^{-2} and 1×10^{15} W cm^{-2} for both 532 nm and 1064 nm lasers. Such an analysis of several interrelated time-dependent density-based quantities for molecules under intense laser fields does not appear to have been reported before.

3.1 Contour plots of electron density

Contour plots of the electron density of H_2 for $\lambda = 532$ and 1064 nm have been depicted in Figures 1−3, for different times and laser intensities. These provide a detailed visualization of the geometrical nature of changes in the electron density in the binding and antibinding regions [53]

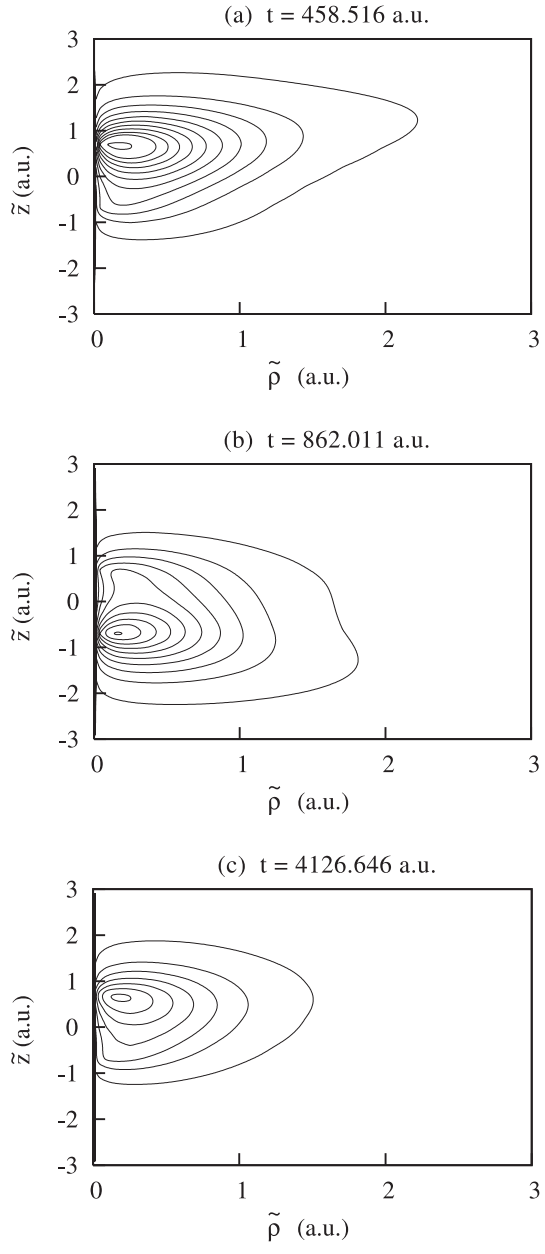

Fig. 2. Contours of time-dependent density (a.u) in the plane $(\tilde{\rho}, \tilde{z})$ for $\lambda = 532$ nm and $I = 1 \times 10^{15}$ W cm^{-2} at (a) $t = 458.516$, (b) $t = 862.011$, (c) $t = 4126.646$ a.u. The total interaction time is 100 fs, i.e., 4134.1276 a.u.

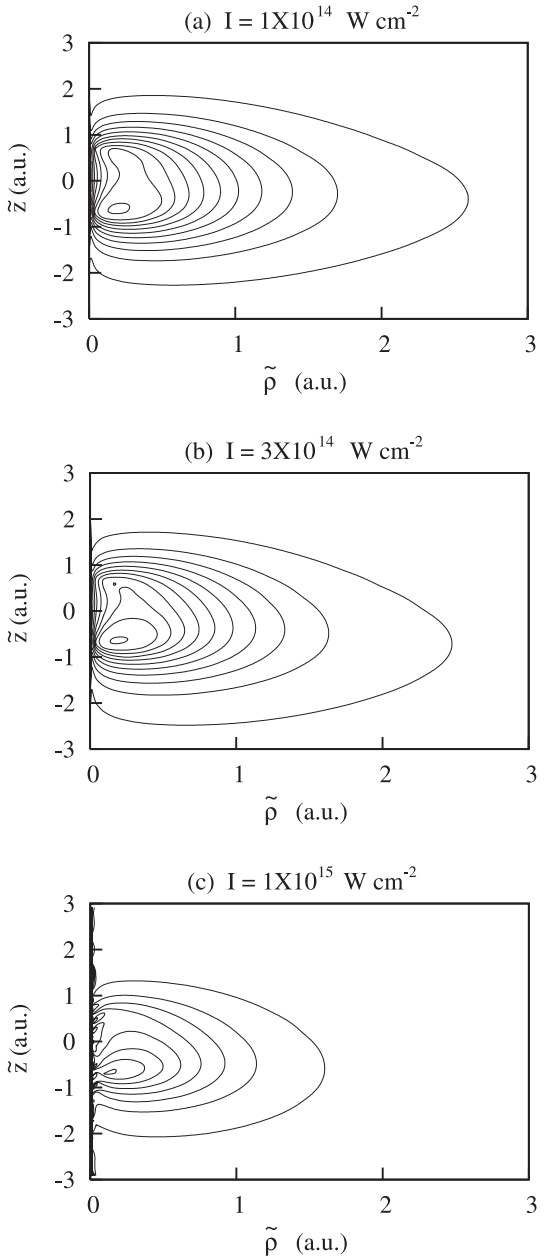

Fig. 3. Contours of time-dependent density (a.u) in the plane $(\tilde{\rho}, \tilde{z})$ for $\lambda = 1064$ nm and $t = 4071.624$ a.u for (a) $I = 1\times10^{14}$, (b) $I = 3\times10^{14}$, (c) $I = 1\times10^{15}$ W cm^{-2}. The total interaction time is 100 fs, i.e., 4134.1276 a.u.

thereby yielding additional insights into the phenomena of bond softening, excitation and consequent dissociation. The internal consistency of the pictures and their interpretations below constitute a valuable check on the numerical accuracy of our algorithm for both imaginary-time and real-time evolution.

Initially ($t = 0$), for $\lambda = 532$ nm, the electron density is symmetric around the two protons A and B as well as in the overlap region so that there is no net force [53] exerted on any proton in the equilibrium configuration (Fig. 1a). With the onset of the laser field, the density acquires as asymmetry except when the oscillating laser field vanishes at $t = n\pi/\omega_L$, $n = 0, 1, 2, \ldots$ At $t = 458.52$ a.u (laser field at a maximum), density is accumulated around proton A and depleted around proton B (Fig. 1b), thereby creating two unequal "halves" of the molecule which respond differently to the laser field. At $t = 862.01$ a.u (laser field at a minimum), the situation is reversed so that density is now depleted around proton A and accumulated around proton B (Fig. 1c). Thus, the TD electron density fluctuates in response to the sign and magnitude of the laser field. This feature persists all through the laser-molecule interaction, e.g., at the trough ($t = 4089.97$ a.u; Fig. 1d), the crest ($t = 4126.65$ a.u; Fig. 1f) and the vanishing field

in between (t = 4108.3 a.u; Fig. 1e) of the last optical cycle. A comparison of Figures 1c and 1d, 1b and 1f, as well as Figures 1a and 1e indicates the internal consistency and the accuracy of the present calculations. Thus, the initially nonpolar H_2 molecule oscillates between the polar $H_A^{\delta+}H_B^{\delta-}$ and $H_A^{\delta-}H_B^{\delta+}$ species. Such polarization increases at higher laser intensities with the density becoming more asymmetric (Fig. 2), thereby closely resembling an $H_A^+H_B^-$ or $H_A^-H_B^+$ situation, indicating greater ionization compared to those for lower intensities. Such localized bound states are created in an intense laser field and these should be involved in the mechanism of non-sequential double ionization [30]. An understanding of this would help in visualizing how electron correlation and molecular structure affect each other dynamically when exposed to strong fields. The contour plots also show that the two nuclei have drawn more electronic charge towards themselves in a dissimilar manner at the expense of electron density from the overlap region. Thus, both the nuclei tend to get back the electron density they contributed for the bond formation in H_2 indicating bond-softening being a precursor of dissociation. In other words, bond softening occurs by an unequal (asymmetric) electron distribution around the two nuclei whereby the molecule becomes instantaneously polar. A comparison between Figure 1a and any of Figures 1b−1f clearly reveals that, at any time, the electron densities near the nuclei and in the region between them are respectably higher and lower compared to those at $t = 0$ (see also Sect. 3.3).

The features discussed above for the 532 nm laser are representative of those for other intensities and for the 1064 nm laser. Figure 3 for $\lambda = 1064$ nm shows a gradual depletion of density at higher intensities and the spread along $\tilde{z}$ is also observed for the highest intensity (Fig. 3c).

3.2 Difference density

The difference density at $t = 0$ is calculated as [49]

$$\Delta\rho\,(\tilde{\rho},\tilde{z},0) = \rho_{H_2}\,(\tilde{\rho},\tilde{z},0) - \{\rho_{H_A}(\tilde{\rho},\,-R_{eq}/2) + \rho_{H_B}(\tilde{\rho},\,R_{eq}/2)\} \quad (12)$$

where $\rho_{H_2}\,(\tilde{\rho},\tilde{z},0)$ is the molecular density at $t = 0$ obtained from the imaginary-time calculation (Fig. 4a). ρ_{H_A} and ρ_{H_B} are the densities of two non-interacting hydrogen atoms placed at the same equilibrium internuclear distance as in the H_2 molecule. The significance of difference density is that it gives an idea of the stability of the molecule and indicates how and where density changes occur when two atoms interact and form a chemical bond resulting in the formation of a molecule [54]. As shown in the perspective plot in Figure 4b, density is significantly built up in the binding [53,55] region between the nuclei as should occur on bond formation and gets depleted in the antibinding [53,55] regions.

The time-dependent difference density is calculated as

$$\Delta\rho_t\,(\tilde{\rho},\tilde{z},t) = \rho_{H_2}\,(\tilde{\rho},\tilde{z},t) - \rho_{H_2}\,(\tilde{\rho},\tilde{z},0)\,. \quad (13)$$

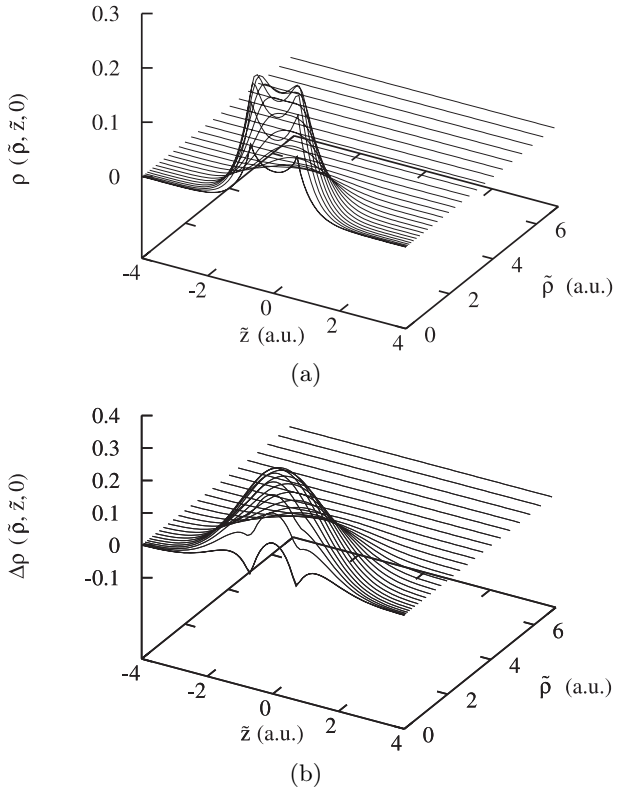

Fig. 4. Perspective plots (a.u) of initial (a) density, $\rho\,(\tilde{\rho},\tilde{z},0)$ and (b) difference density $\Delta\rho\,(\tilde{\rho},\tilde{z},0)$ in the $(\tilde{\rho},\tilde{z})$-plane.

This quantity reveals the dynamical reorganization of electron density as a result of laser-molecule interaction. A negative or positive difference density implies that density is getting depleted or accumulated respectively in certain regions of space as compared to the molecular density at $t = 0$. Figure 5 clearly shows that density is depleted in the regions near the two nuclei indicating that density has moved away from the binding region resulting in a negative difference density. There is also an accumulation of density in the antibinding regions somewhat far from the nuclei giving rise to a positive difference density. A combination of these two effects, viz. depletion in the binding region and accumulation in the antibinding region, is likely to be the main reason for Coulomb explosion. Figure 5 also shows that the overlap region is becoming poorer in density and there is a spread of density along $\tilde{z}$ and $\tilde{\rho}$-directions. The positive regions are thus concentrated along both $\tilde{z}$ and $\tilde{\rho}$, mostly well outside the negative regions. The left-right asymmetry of the positive regions is also seen in the plot, again depending on the switching of direction of the laser field. While the positive region almost reaches the periphery of the computation grid in the $\tilde{z}$-direction, it never reaches the periphery in the $\tilde{\rho}$-direction. However, the values of positive $\Delta\rho_t$ are small as compared to negative $\Delta\rho_t$ indicating that the depletion of density is more than its accumulation signifying bond-softening, bond-breaking and ionization.

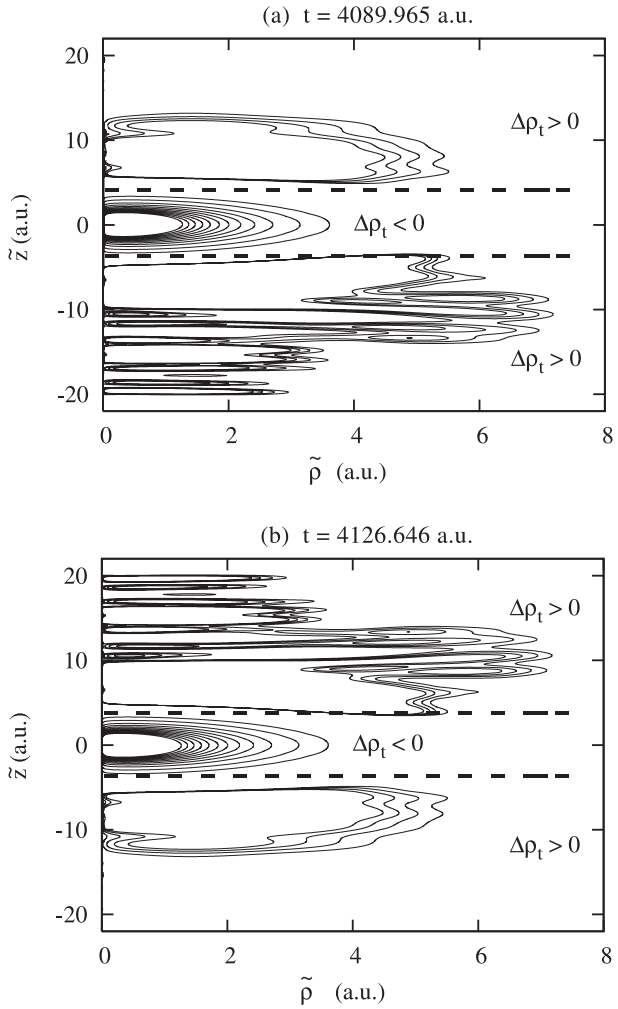

Fig. 5. Contours of time-dependent difference density (a.u), $\Delta\rho\,(\tilde{\rho},\tilde{z},t)$ for $\lambda = 532$ nm and $I = 1\times10^{15}$ W cm^{-2} at (a) $t =$ 4089.965, (b) $t = 4126.646$ a.u. The negative difference density range is approximately $-3 \leq \tilde{z} \leq 3$. Positive regions are outside this range and correspond to greater density accumulation. The thick dashed lines indicate vanishing difference density. The total interaction time is 100 fs, i.e., 4134.1276 a.u.

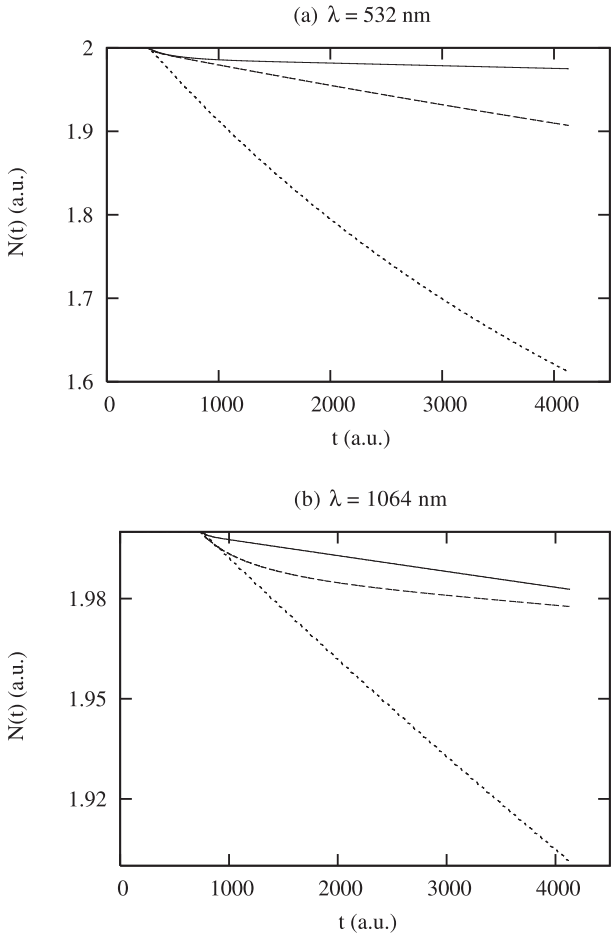

Fig. 6. Time-dependent electronic charge (a.u), $N(t)$ for (a) $\lambda = 532$ nm and (b) $\lambda = 1064$ nm. The uppermost line is for $I = 1\times10^{14}$, the middle one for $I = 2\times10^{14}$ and the lowest one for $I = 3\times10^{14}$ W cm^{-2} respectively.

3.3 Electronic charges around different regions and ionization rates

One of the most important mechanisms of decay in atoms and molecules is through ionization which, in case of molecules, may be preceded by dissociation and/or Coulomb explosion. An analysis of ionization rates is therefore not only necessary to understand the decay dynamics, it is also an important tool to predict the efficiency of systems for high harmonics generation. Here, we present an analysis of electronic charges around different regions, calculate ionization rates and compare with the existing literature.

The total electronic charge $N(t)$ is calculated as

$$N\,(t) = \int_0^{2\pi}\int_0^{\tilde{\rho}}\int_{-z_{\max}}^{z_{\max}} \rho\,(\tilde{\rho},\tilde{z},t)\tilde{\rho}\;d\tilde{z}\;d\tilde{\rho}\;d\tilde{\phi} \qquad (14)$$

$N(t) = 2$ at $t = 0$. The calculation of $N(t)$ at different times indicates the progress of ionization with time (Fig. 6). For simplicity, we have calculated the ionization rate as $[N(0) - N(t)]/t$, where t denotes the duration (100 fs) of the interaction. This amounts to approximating the ionization curves in Figure 6 by straight lines instead of an exponential function whose decay constant is the ionization rate.

We have also calculated the charges in the other regions, namely, binding region, N_{BR} and in the two antibinding regions, N_A^{LS} and N_B^{RS} while N_A and N_B are the

Table 1. $N(t)$ values and ionization rates for H_2 molecule interacting with lasers of $\lambda = 532$ and 1064 nm.

λ (nm)	I (W cm^{-2})	$N(t)$ at 100 fs	Ionization rate (s^{-1})
532	1×10^{14}	1.9749	2.505×10^{11}
	3×10^{14}	1.6117	3.883×10^{12}
	1×10^{15}	0.58	1.42×10^{13}
1064	1×10^{14}	1.9776	2.24×10^{11}
	3×10^{14}	1.9013	9.87×10^{11}
	1×10^{15}	0.708	1.292×10^{13}

charges in the regions of A and B protons, as follows [44]:

$$N_A(t) = \int_0^{2\pi}\int_0^{\tilde{\rho}}\int_{-\tilde{z}_{\max}}^{0} \rho(\tilde{\rho},\tilde{z},t)\tilde{\rho}\, d\tilde{z}\, d\tilde{\rho}\, d\tilde{\phi} \tag{15a}$$

$$N_B(t) = \int_0^{2\pi}\int_0^{\tilde{\rho}}\int_{0}^{\tilde{z}_{\max}} \rho(\tilde{\rho},\tilde{z},t)\tilde{\rho}\, d\tilde{z}\, d\tilde{\rho}\, d\tilde{\phi} \tag{15b}$$

$$N_{BR}(t) = \int_0^{2\pi}\int_0^{\tilde{\rho}}\int_{\tilde{z}=-0.7035}^{\tilde{z}=0.7035} \rho(\tilde{\rho},\tilde{z},t)\tilde{\rho}\, d\tilde{z}\, d\tilde{\rho}\, d\tilde{\phi} \tag{16}$$

$$N_A^{LS}(t) = \int_0^{2\pi}\int_0^{\tilde{\rho}}\int_{-\tilde{z}_{\max}}^{\tilde{z}=-0.7035} \rho(\tilde{\rho},\tilde{z},t)\tilde{\rho}\, d\tilde{z}\, d\tilde{\rho}\, d\tilde{\phi} \tag{17a}$$

$$N_B^{RS}(t) = \int_0^{2\pi}\int_0^{\tilde{\rho}}\int_{\tilde{z}=0.7035}^{\tilde{z}_{\max}} \rho(\tilde{\rho},\tilde{z},t)\tilde{\rho}\, d\tilde{z}\, d\tilde{\rho}\, d\tilde{\phi}. \tag{17b}$$

We now analyze the above quantities during the course of interaction of the molecule with the laser field (see also Sect. 3.1). Note that the above definitions take the boundary surfaces separating the binding and antibinding regions as rectangular/plane surfaces instead of the actual hyperboloid surfaces.

Figure 6 shows that $N(t)$ has a constant value of 2 up to the time when the ramp is employed and the electric field reaches its maximum. Thereafter, a reduction in $N(t)$ is observed the extent of which depends on the laser intensity (or the strength of laser field) as shown in the following Table 1. Thus, for $\lambda = 532$ nm, the per cent decrease in $N(t)$ goes from 1.25 for $I = 1\times10^{14}$ W cm^{-2} to 71 for $I = 1 \times 10^{15}$ W cm^{-2} expectedly indicating a drastic increase in the ionization rate for the latter intensity. A similar conclusion holds for the 1064 nm laser where the per cent decrease goes from 1.12 for $I = 1 \times 10^{14}$ W cm^{-2} to 64.6 for $I = 1 \times 10^{15}$ W cm^{-2}.

Table 1 reports the $N(t)$ values for both the lasers at different intensities. The ionization rate at $\lambda = 532$ nm and 1×10^{14} W cm^{-2} intensity is reported [20] as 2.5×10^{11} s^{-1}, which shows that there is an excellent matching between the value obtained by our calculation and the literature value. The ionization rate for $\lambda = 1064$ nm and 1×10^{14} W cm^{-2} intensity also agrees with that reported by Yu et al. [22]. However, the values obtained here for the higher intensities are somewhat less than the values reported diagrammatically by these authors indicating greater ionization in the present case.

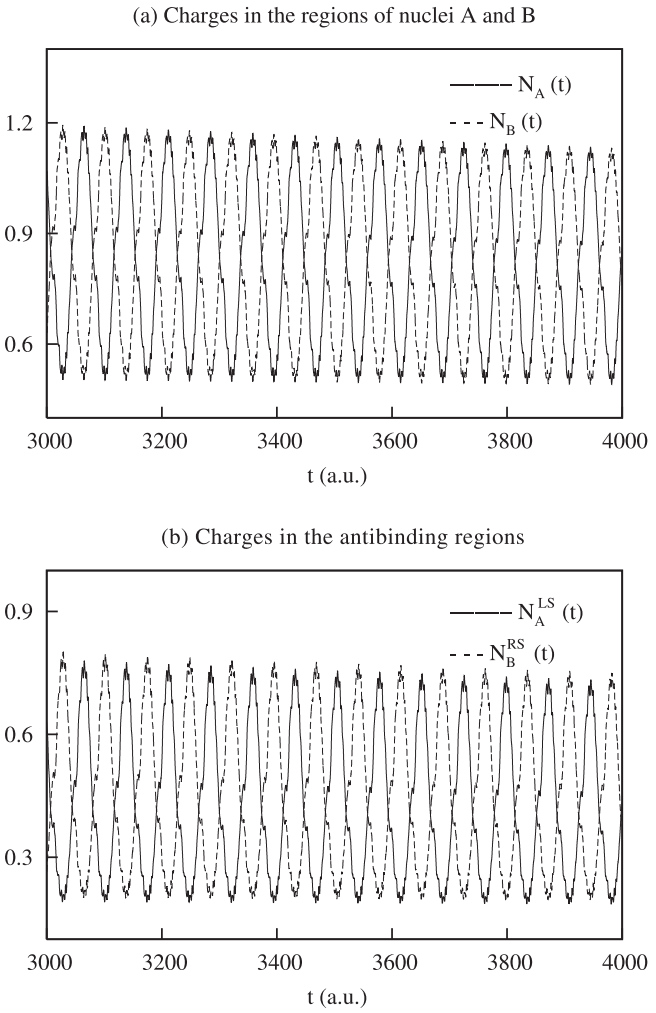

Fig. 7. Time-dependent electronic charge (a.u) in the regions of (a) nuclei A and B, (b) in the antibinding regions for $\lambda = 532$ nm and $I = 3 \times 10^{14}$ W cm^{-2}. Similar qualitative features are observed for other intensities and for $\lambda = 1064$ nm. In (a), the first peak corresponds to $N_B(t)$ while the first trough corresponds to $N_A(t)$. In (b), the first peak corresponds to $N_B^{RS}(t)$ while the first trough corresponds to $N_A^{LS}(t)$. At $t = 0$, $N_A(t) = N_B(t) = 1.0$.

An analysis of charges on both the protons, between them and beyond them also supports the findings from the contour plots of electron density and the difference density (Sects. 3.1, 3.2). The picture of charges on the two nuclei (Fig. 7a) is a clear evidence of asymmetric charge distribution on the nuclei depending on the sign and strength of the laser field. Initially ($t = 0$), the charges on both nuclei are the same. With the onset of the laser field, N_A starts increasing and N_B starts decreasing. When the laser field is at its maximum, the density has moved towards

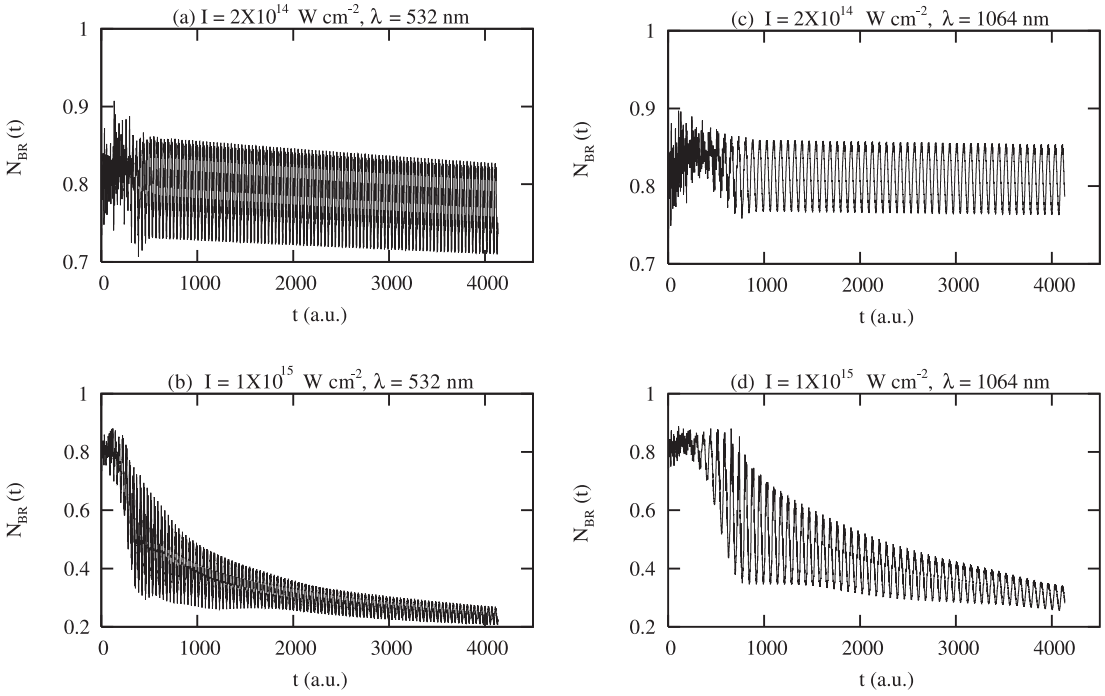

Fig. 8. Time-dependent electronic charge (a.u) in the binding regions, $N_{BR}(t)$ for $\lambda = 532$ nm and (a) $I = 2 \times 10^{14}$ W cm^{-2}, (b) $I = 1 \times 10^{15}$ W cm^{-2}. Similar features are observed for $\lambda = 1064$ nm and (c) $I = 2 \times 10^{14}$ W cm^{-2}, (d) $I = 1 \times 10^{15}$ W cm^{-2}.

nucleus A and nucleus B is partially deprived of its density indicating the formation of $H_A^{\delta-} H_B^{\delta+}$. Thereafter, the field strength starts decreasing and nucleus B starts regaining its lost electron density. When the field vanishes, the two nuclei regain their equal share of density (see also Fig. 1e). At the minima of the electric field, nucleus B is richer in density indicating the formation of $H_A^{\delta+}$ $H_B^{\delta-}$ and this process of the density swinging back and forth between the two nuclei repeats itself in each optical cycle with the charge maximum for H_A coinciding with the charge minimum for H_B and vice versa (Fig. 7a). This asymmetric charge distribution is the result of different effective potentials experienced by the electrons for the two nuclei in the presence of the external field. During the first half of the laser field, V_{ext} is negative along the positive $\tilde{z}$-axis; therefore, density swings to the region of B nucleus. This swinging of density between the positive and negative $\tilde{z}$-directions has the same periodicity as that of the laser field. For the first five optical cycles (when the ramp is not yet crossed), the total number of electrons remains 2; thereafter ionization starts at a rate depending on the laser intensity. Consequently, the charges on atoms also decrease to a greater extent for higher intensities as compared to lower intensities.

A closer examination of the total density behind the nuclei, i.e., the antibinding regions (Fig. 7b) and in between the nuclei, i.e., the binding region (Fig. 8) provides evidence of bond-softening as well as ionization. There is an overall decrease of density in the binding region (Fig. 8) implying a softening of the H−H bond. Such removal of density from the binding region takes place in a non-symmetric manner which means that the instantaneous states of the two H "atoms" become different in the H_2 molecule as interaction progresses. The extent of this reduction in density or bond-softening depends on the laser field strength, i.e., the laser intensity. For instance, the minimum value of N_{BR} is 0.85 for $I = 1 \times 10^{14}$ W cm^{-2} and 532 nm laser as compared to 0.27 for $I = 1 \times 10^{15}$ W cm^{-2} where density almost disappears from the binding region. One can also gauge the asymmetric charge distribution between the two nuclei from the charges calculated in the regions behind the two nuclei. Here too, as the density on the left side of nucleus A increases, that on the right side of nucleus B decreases with the overall density in both the regions decreasing during the interaction. This also gives a clear indication of ionization. The same qualitative features are also valid for the 1064 nm laser.

In the light of the above observations, we conclude that (i) bond-softening occurs when the molecule interacts with the laser field; (ii) an asymmetric electron distribution between the two nuclei takes place, making the molecule instantaneously polar; (iii) the asymmetric charge distribution indicates that the two "atoms" enter different states as the interaction progresses, a considerable part of the molecular density corresponding to higher repulsive states from where ionization and dissociation can readily occur; (iv) the electronic charges in different regions change with time in phase with the laser field.

3.4 Ground-state survival probability

The ground-state survival probability, a measure of the contribution of ground state to the total probability

Table 2. Ground-state survival probabilities for lasers with $\lambda = 532$ and 1064 nm, at different intensities and times (t_0 denotes the completion of ramp).

λ (nm)	I (W cm^{-2})	$P_{gs}(t = t_0)$	$P_{gs}(t = 100$ fs)
532	1×10^{14}	0.85	0.8
	2×10^{14}	0.815	0.78
	3×10^{14}	0.795	0.69
	1×10^{15}	0.64	0.26
1064	1×10^{14}	0.859	0.8
	2×10^{14}	0.829	0.8
	3×10^{14}	0.81	0.78
	1×10^{15}	0.78	0.34

density at a given time, is given by

$$P_{gs}(t) = |\langle\Psi(0)|\Psi(t)\rangle|^2 \tag{18}$$

where $P_{gs}(t)$ is normalized to unity at $t = 0$. The excitation and ionization probability (P_{ei}) is defined as

$$P_{ei}(t) = 1 - P_{gs}(t). \tag{19}$$

Table 2 lists the $P_{gs}(t)$ values against different intensities at $t = 8.872$ fs, i.e., at the completion of the ramp and at 100 fs. The initial decrease in the P_{gs} value from unity until the completion of the ramp can be attributed to the redistribution of electron density in the binding/antibinding regions and consequent excitation to higher electronic states where the two hydrogen "atoms" are in different states. This implies that the contributions of higher excited states to the probability density increase with time and these states come into picture sooner for higher intensities. The same applies to the case of 1064 nm laser with per cent decrease of ground-state survival probability for each intensity less than that at the respective intensity for 532 nm laser (Fig. 9).

A comparison of per cent decreases in survival probability and ionization rate reveals that the probability for excitation is more than that of ionization, especially in the first few optical cycles and at lower intensities; the two processes go hand in hand at later times and higher intensities.

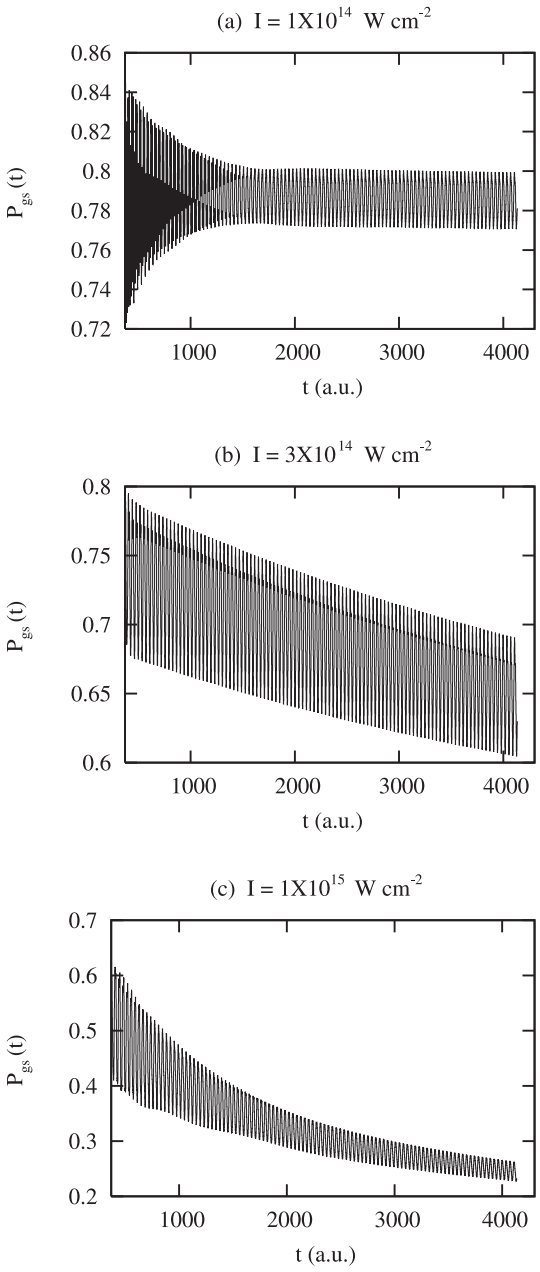

Fig. 9. Ground state survival probability, $P_{gs}(t)$ for $\lambda = 532$ nm and (a) $I = 1 \times 10^{14}$, (b) $I = 3 \times 10^{14}$, (c) $I = 1 \times 10^{15}$ W cm^{-2}.

3.5 Time-dependent dipole moment, $\mu_{\tilde{z}}(t)$

Since the laser field is along the $\tilde{z}$-direction (internuclear axis), the expectation value of the time-dependent dipole moment is given by

$$\mu_{\tilde{z}}(t) = \int \rho\,(\tilde{\rho}, \tilde{z}, t)\tilde{z}\ \tilde{\rho}\ d\tilde{\rho}\ d\tilde{z}\ d\tilde{\phi}. \tag{20}$$

In Figure 10 we have plotted $\mu_{\tilde{z}}(t)$ vs. time t (a.u) for the 532 nm laser (qualitative features remain the same for the 1064 nm laser) and the intensity range $1 \times 10^{14} \leq I \leq 1 \times 10^{15}$ W cm^{-2}; the time-dependent electric field is shown in Figure 11. Upon interaction with the laser field, an oscillating dipole moment is induced as the field strength increases with both quantities completing the same number of oscillations and the maximum of dipole moment coinciding with the maximum of the laser field. Indeed, both reach their maxima at the completion of the ramp. Thereafter, the electric field oscillates between its maximum ($+E_0$) and minimum ($-E_0$) whereas the dipole moment plots show a damping due to ionization. The extent of damping depends on the ionization rate which in turn depends on the laser intensity, i.e., the higher the intensity of the laser, the faster is the ionization, and consequently $\mu_{\tilde{z}}(t)$ shows more damping. This implies that the high intensity laser makes the molecule highly polar and hence

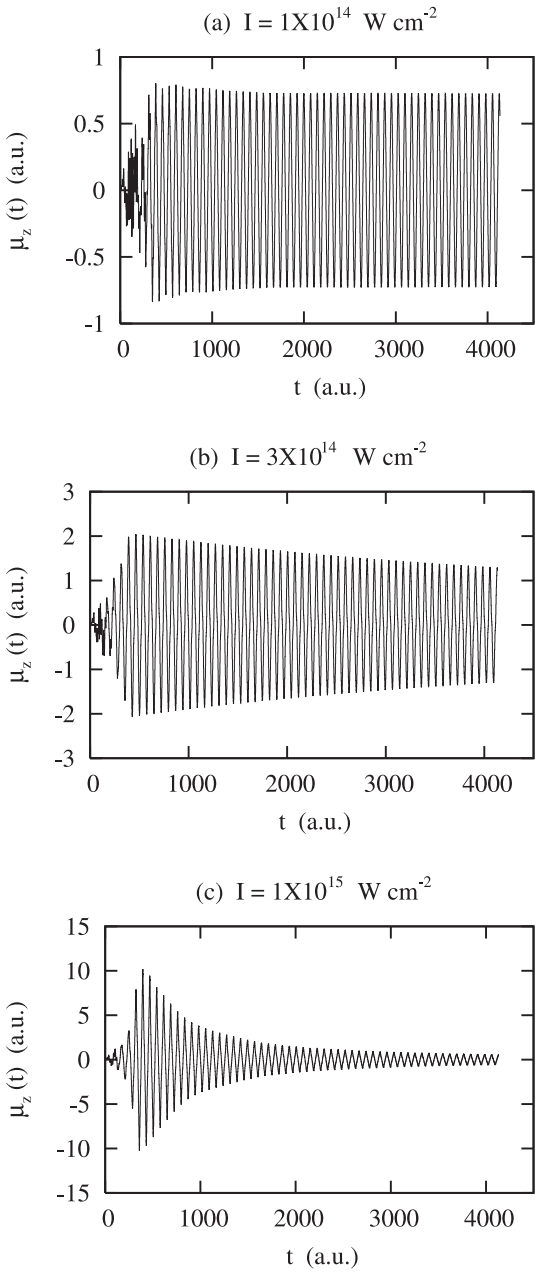

Fig. 10. Time-dependent dipole moment, $\mu_{\tilde{z}}(t)$, in a.u, for $\lambda = 532$ nm and (a) $I = 1 \times 10^{14}$, (b) $I = 3 \times 10^{14}$, (c) $I = 1 \times 10^{15}$ W cm^{-2}.

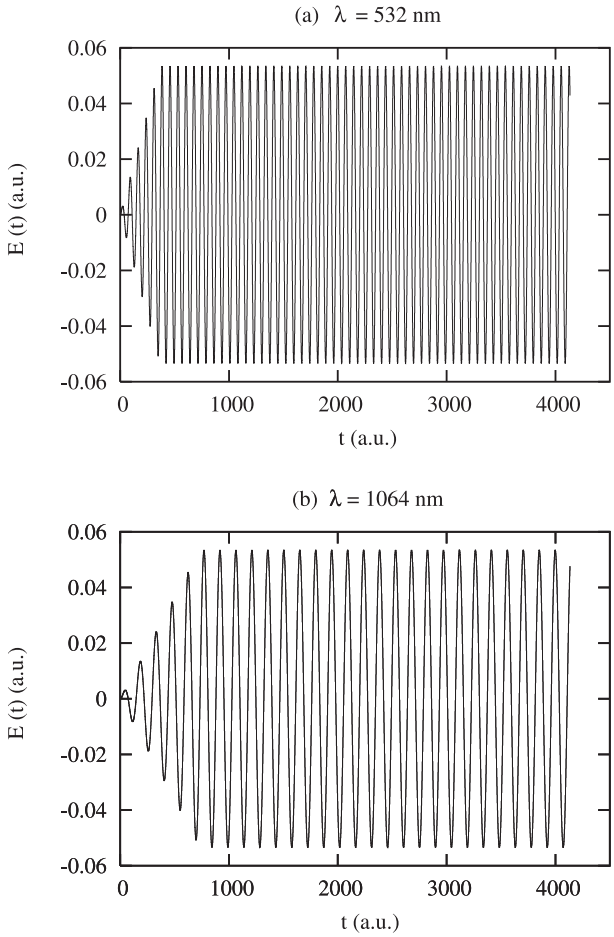

Fig. 11. Time-dependent laser electric field, $E(t)$, in a.u, for $I = 1 \times 10^{14}$ W cm^{-2} and (a) $\lambda = 532$ nm, (b) $\lambda = 1064$ nm.

prone to higher excitations and ionization. At the highest intensity ($I = 1 \times 10^{15}$ W cm^{-2}) considered in the present study, there is considerable damping with the dipole moment after 100 fs reduced to just 10 per cent of its value at the completion of the ramp (Fig. 10c).

3.6 High harmonics generation (HHG)

Atoms and molecules irradiated by an intense laser light emit high order harmonics of the intense field as a result of nonlinear, non-perturbative interaction of the electrons with the intense radiation field and the ion core. Depending on the incident intensity, the spectrum may extend up to very high harmonics. In particular, an extended range of harmonics, forming a plateau, is obtained that consists of peaks with comparable intensities. The harmonic radiation has unique characteristics such as good spatial and temporal coherence, high brightness and ultrashort duration that are primarily responsible for its utility in generating attosecond pulses and novel sources of coherent light with unprecedented properties. The physics is based on a quasiclassical "three-step model" whereby an electron leaves the atom and enters the continuum with zero initial velocity, gets accelerated by the strong electric field, gains energy and is then driven back into the vicinity of the parent ion or a neighbouring ion in a molecule resulting in its recombination to the ground state and emission of a high-frequency photon. Such harmonic generations involve electronic transitions which are much faster than nuclear motions so that vibrational and rotational motions would not significantly alter the features of this phenomenon.

The numerical procedure for obtaining HHG spectrum involves calculating the fast Fourier transform (FFT) of the time-dependent induced dipole moment, $|D(\omega)|^2$, over the last half of the interaction period, against the

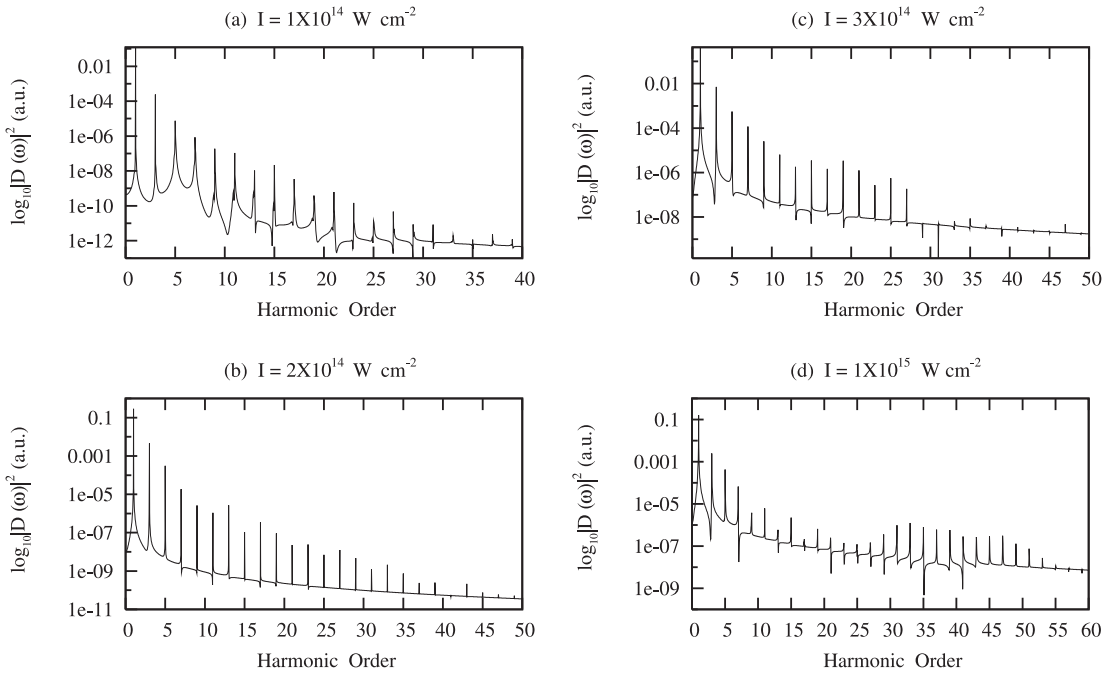

Fig. 12. HHG spectra (a.u) for $\lambda = 532$ nm and (a) $I = 1 \times 10^{14}$, (b) $I = 2 \times 10^{14}$, (c) $I = 3 \times 10^{14}$, (d) $I = 1 \times 10^{15}$ W cm^{-2}.

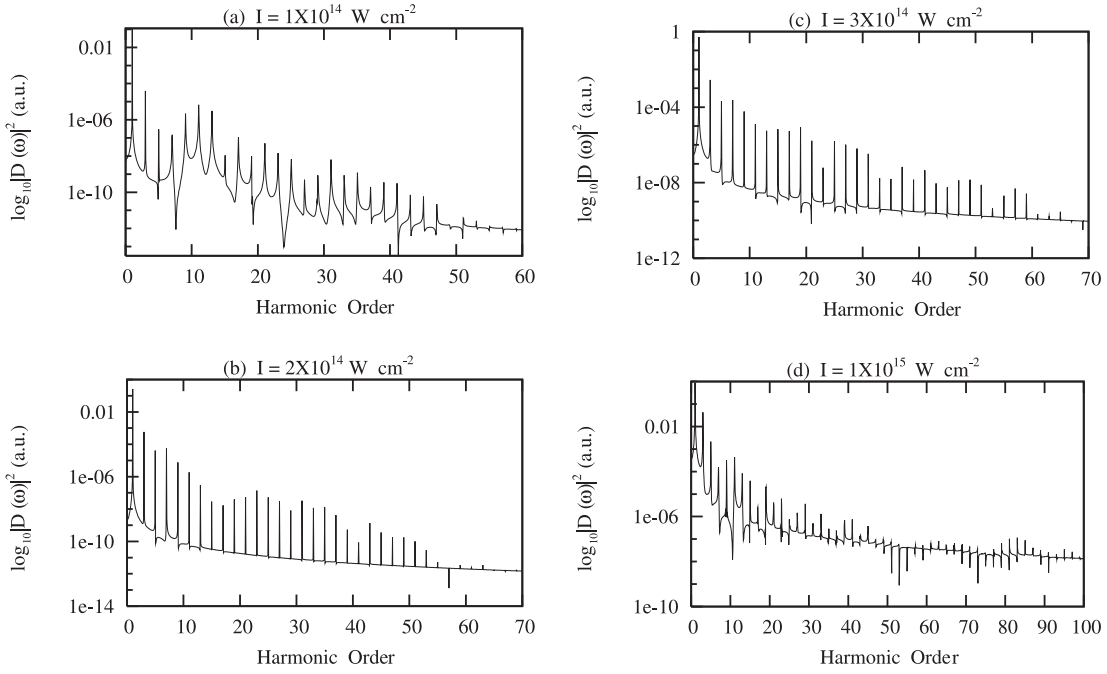

Fig. 13. HHG spectra (a.u) for $\lambda = 1064$ nm and (a) $I = 1 \times 10^{14}$, (b) $I = 2 \times 10^{14}$, (c) $I = 3 \times 10^{14}$, (d) $I = 1 \times 10^{15}$ W cm^{-2}.

harmonic order (ω/ω_L). Figures 12 and 13 present the harmonic spectra obtained for H_2 molecule for $\lambda = 532$ and 1064 nm as well as varying intensities from 1×10^{14} to 1×10^{15} W cm^{-2}. Each spectrum reveals a series of peaks placed at odd multiples of the incident laser frequency due to the generation of frequency components of dipole moment at those multiples of laser frequency. HHG spectra obtained in the present study are in excellent agreement with the diagrammatic information reported in the literature [20,22], regarding the number and yields of the harmonics, and display their characteristic features, namely, a sharp decline in the intensities of harmonics for the first few harmonics, followed by a plateau of harmonics with comparable intensities and then a cut-off. The plateau extends to higher harmonics at larger intensities as observed for both 532 and 1064 nm lasers. Such high order harmonic generation is a promising way to generate coherent X-rays and to produce attosecond XUV and

soft X-ray pulses [56,57]. Methods for achieving selectivity of harmonics as well as controlling HHG constitute an important research area.

4 Conclusion

To summarize, the results discussed above demonstrate the interrelated phenomena of excitation, ionization, bond-softening and/or dissociation by the following observations: (i) both the nuclei lose electron density from their respective regions; (ii) electron density is depleted in the binding region; (iii) the two antibinding regions (one to the left of nucleus A and the other to the right of nucleus B) possess different density distributions, making the molecule instantaneously polar; (iv) the asymmetric distributions of charge surrounding the two individual nuclei make the states of the two "atoms" different in the perturbed molecule; (v) a time-dependent dipole moment is induced in the molecule that has the same periodicity as the laser electric field and shows damping depending on the laser intensity (note that it is not necessary that the dipole moment should have the periodicity of the driving field, see e.g., NO molecule modeled as a Morse oscillator [58]); (vi) high order harmonics are obtained as a result of generation of frequency components of induced dipole moment at odd multiples of incident laser frequency.

The principal objective of our work on H_2 molecule under intense laser field was to demonstrate that the TD QFDFT method is a suitable and powerful technique to study laser-molecule interactions. Although our study is restrained by the Born-Oppenheimer approximation and is limited to the equilibrium internuclear distance $R_{eq} = 1.4$ a.u, its importance lies in the information and insights it provides by following the dynamics of electron density over different regions of the molecule including the antibinding regions. Moreover, a full treatment of the three-dimensional electronic motion allows us to readily visualize the spread along $\tilde{z}$ and $\tilde{\rho}$-directions and its consequences that is not possible with one-dimensional studies. Furthermore, the numerical method permits, in principle, the calculation of density to *all orders of change*. The dependence of dynamical evolution on laser parameters is also extensively studied by employing lasers of two wavelengths 532 and 1064 nm over a range of intensities from $I = 1 \times 10^{14}$ to 1×10^{15} W cm^{-2}. To the best of our knowledge, such an analysis of time-dependent density-based quantities for molecule-laser interactions has not been done earlier. The results obtained are not only in excellent agreement with the available literature, they are consistent with one another and can also be understood from a density viewpoint. Thus, interesting insights have been obtained into molecular time-dependent phenomena such as excitation, ionization, bond-softening, dipole-formation, high harmonics generation, etc. from movements of the electron cloud. In principle, it should also be possible to examine molecular dissociation by solving two *coupled* equations of motion, one being an equation of motion for the electron density and the other being a classical equation of motion for the nuclei which employs the TD electron density as a feedback. The present method thus appears quite promising for studying time-dependent phenomena involving molecules which can yield attractive and transparent physical insights into such dynamical processes.

A.W. thanks the C.S.I.R., New Delhi, for financial support and Prof. Ramesh Kapoor for creating the necessary computer facilities.

References

1. *Molecules in Laser Fields*, edited by A.D. Bandrauk (Dekker, New York, 1994)
2. J.H. Posthumus, Rep. Prog. Phys. **67**, 623 (2004)
3. B. Sheehy, Annu. Rep. Prog. Chem. Sect. C **97**, 383 (2001)
4. C.R. Scheper, W.J. Buma, C.A. de Lange, W.J. van der Zande, J. Chem. Phys. **109**, 8319 (1998)
5. J. Khatun, K.R. Dastidar, J. Phys. B: At. Mol. Opt. Phys. **32**, 373 (1999)
6. P. Agostini, F. Fabre, G. Mainfray, G. Petite, N.K. Rahman, Phys. Rev. Lett. **42**, 1127 (1979)
7. J.H. Eberly, J. Javanainen, K. Rzazewski, Phys. Rep. **204**, 331 (1991)
8. C. Cornaggia, D. Dormand, J. Morellec, G. Mainfray, C. Manus, Phys. Rev. A **34**, 207 (1986)
9. J.W.J. Verschur, L.D. Noordham, H.B. van Linden van der Heuvell, Phys. Rev. A **40**, 4383 (1989)
10. P.H. Bucksbaum, A. Zavriyev, H.G. Muller, D.W. Schumacher, Phys. Rev. Lett. **64**, 1883 (1990)
11. A.D. Bandrauk, J.M. Gauthier, E. Constant, J. Opt. Soc. Am. B **7**, 1422 (1990)
12. J.J. Larsen, I. Wendt-Larsen, H. Stapelfeldt, Phys. Rev. Lett. **83**, 1123 (1999)
13. X.X. Zhou, X.M. Tong, Z.X. Zhao, C.D. Lin, Phys. Rev. A **71**, 061801R (2005)
14. A. McPherson, G. Gibson, H. Jara, U. Johann, T.S. Luk, I.A. McIntyre, K.B. Uyer, C.K. Rhodes, J. Opt. Soc. Am. B **4**, 595 (1987)
15. A. L'Huillier, K.J. Schafer, K.C. Kulander, J. Phys. B **24**, 3315 (1991)
16. P. Salieres, A. L'Huillier, P. Antoine, M. Lewenstein, Adv. At. Mol. Phys. **41**, 83 (1999)
17. A.D. Bandrauk, S. Chelkowski, H.Y. Lu, Riken Rev. **29**, 55 (2000)
18. V. Averbukh, O.E. Alon, N. Moiseyev, Phys. Rev. A **64**, 033411 (2001)
19. X. Chu, S.-I. Chu, Phys. Rev. A **63**, 023411 (2001)
20. H. Yu, A.D. Bandrauk, J. Chem. Phys. **102**, 1257 (1995)
21. A.D. Bandrauk, H. Lu, J. Phys. B: At. Mol. Opt. Phys. **38**, 2529 (2005)
22. H. Yu, T. Zuo, A.D. Bandrauk, Phys. Rev. A **54**, 3290 (1996)
23. A. Saenz, Phys. Rev. A **61**, 051402(R) (2000)
24. A. Zavriyev, P.H. Bucksbaum, H.G. Muller, D.W. Schumacher, Phys. Rev. A **42**, 5500 (1990)
25. A. Saenz, Phys. Rev. A **66**, 063407 (2002)
26. K. Codling, L.J. Fransinski, J. Phys. B **26**, 783 (1993)
27. M. Schmidt, D. Normand, C. Cornaggia, Phys. Rev. A **50**, 5037 (1994)

28. E. Constant, H. Stapelfeldt, P.B. Corkum, Phys. Rev. Lett. **76**, 4140 (1996)
29. I. Kawata, H. Kono, Y. Fujimara, A.D. Bandrauk, Phys. Rev. A **62**, 031401 (2000)
30. K. Harumiya, H. Kono, Y. Fujimara, I. Kawata, A.D. Bandrauk, Phys. Rev. A **66**, 043403 (2002)
31. M. Lein, T. Kreibich, E.K.U. Gross, V. Engel, Phys. Rev. A **65**, 033403 (2002)
32. A. Castro, M.A.L. Marques, J.A. Alonso, G.F. Bertsch, A. Rubio, Eur. Phys. J. D **28**, 211 (2004)
33. D. Dundas, J.Phys. B: At. Mol. Opt. Phys. **37**, 2883 (2004)
34. V.I. Usachenko, S.-I. Chu, Phys. Rev. A **71**, 063410 (2005)
35. S.K. Ghosh, B.M. Deb, Phys. Rep. **92**, 1 (1982)
36. B.M. Deb, S.K. Ghosh, in *The Single Particle Density in Physics and Chemistry*, edited by N.H. March, B.M. Deb (Academic Press, London, 1987)
37. B.M. Deb, S.K. Ghosh, J. Chem. Phys. **77**, 342 (1982)
38. B.M. Deb, P.K. Chattaraj, Phys. Rev. A **39**, 1696 (1989)
39. B.K. Dey, B.M. Deb, Int. J. Quant. Chem. **56**, 707 (1995)
40. B.K. Dey, B.M. Deb, Pramana J. Phys. **48**, L849 (1997)
41. B.K. Dey, B.M. Deb, Int. J. Quant. Chem. **70**, 441 (1998)
42. A.K. Roy, S.-I. Chu, Phys. Rev. A **65**, 043402 (2002)
43. B.K. Dey, B.M. Deb, Chem. Phys. Lett. **276**, 157 (1997)
44. B.K. Dey, *Density Functional and Quantum Fluid Dynamics of Many-Electron Systems*, Ph.D. thesis, Panjab University, Chandigarh, India, 1996
45. B.M. Deb, P.K. Chattaraj, in *Solitons: Introduction and Applications*, edited by M. Lakshmanan (Springer-Verlag, Berlin, 1988)
46. S.K. Ghosh, B.M. Deb, J. Phys. B: At. Mol. Opt. Phys. **27**, 381 (1994)
47. Ranbir Singh, B.M. Deb, Phys. Rep. **311**, 47 (1999)
48. W. Kohn, Rev. Mod. Phys. **71**, 1253 (1999)
49. A.K. Roy, N. Gupta, B.M. Deb, Phys. Rev. A **65**, 012109 (2002)
50. W. Kolos, L. Wolniewicz, J. Chem. Phys. **43**, 2429 (1965)
51. G.D. Smith, *Numerical Solution of Partial Differential Equations* (Oxford University Press, London, 1965)
52. A.R. Mitchell, *Computational Methods in Partial Differential Equations* (John Wiley, London, 1976)
53. B.M. Deb, Rev. Mod. Phys. **45**, 22 (1973)
54. R.F.W. Bader, in *The Force Concept in Chemistry*, edited by B.M. Deb (Van Nostrand-Reinhold, New York, 1981)
55. T. Berlin, J. Chem. Phys. **19**, 208 (1951)
56. A. Wadehra, Vikas, B.M. Deb, J. Chem. Phys. **119**, 6620 (2003)
57. Y. Mairesse, A. de Bohan, L.J. Frasinski, H. Merdji, L.C. Dinu, P. Monchicourt, P. Breger, M. Kovacev, R. Taieb, B. Carré, H.G. Muller, P. Agostini, P. Salières, Science **302**, 1540 (2003)
58. A. Wadehra, B.M. Deb, Proc. Indian Acad. Sci. (Chem. Sci.) **115**, 349 (2003); *erratum*, J. Chem. Sci. **116**, 129 (2004)